ACS MATERIALS Au
AN OPEN ACCESS JOURNAL OF THE AMERICAN CHEMICAL SOCIETY

pubs.acs.org/materialsau
Article

Multinuclear Tin-Based Macrocyclic Organometallic Resist for EUV Photolithography

Gayoung Lim,[‖] Kangsik Lee,[‖] Chawon Koh, Tsunehiro Nishi, and Hyo Jae Yoon*

Cite This: ACS Mater. Au 2024, 4, 468−478
Read Online

ACCESS | Metrics & More | Article Recommendations | Supporting Information

ABSTRACT: We report a new photoresist based on a multinuclear tin-based macrocyclic complex and its performance for extreme UV (EUV) photolithography. The new photoresist has a trinuclear macrocyclic structure containing three salicylhydroxamic acid ligands and six Sn−CH_3 bonds, which was confirmed by multinuclear nuclear magnetic resonance (NMR) and FT-IR spectroscopies and single-crystal X-ray diffraction study. The resist exhibited good humidity, air, and thermal stabilities, while showing good photochemical reactivity. Photochemical cross-linking of the resist was confirmed by X-ray photoelectron and solid-state NMR spectroscopic analyses. EUV photolithography with the 44 nm-thick film on a silicon wafer revealed a line-edge-roughness (LER) of 1.1 nm in a 20 nm half-pitch pattern. The *Z*-factor, a metric that gauges the performance of photoresists by considering the tradeoff between resolution, LER, and sensitivity (RLS), was estimated to be 1.28×10^{-8} mJ·nm^3, indicating its great performance compared to the EUV photoresists reported in the literature.

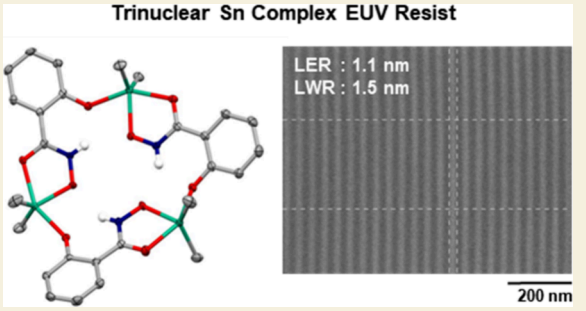

KEYWORDS: *multinuclear tin complex, extreme ultraviolet (EUV), patterning, photoresist, nanometers, lithography*

INTRODUCTION

In the semiconductor industry, the production of improved-performance integrated circuits depends dominantly on the resolution limit in photolithography. Reducing the wavelength of light used in photolithography is imperative for attaining high-resolution patterns, as shorter wavelengths of the light source lead to higher resolution according to Rayleigh's criterion.[1,2] Hence, to attain higher resolution in the process of photolithography, the wavelength of the light source has progressively decreased over time. Recently, photolithography systems based on extreme ultraviolet (EUV) with a wavelength of 13.5 nm have received significant attention for the high-resolution and high-volume manufacturing of integrated circuits by semiconductor chip makers.[2−4] According to the Institute of Electrical and Electronics Engineers (IEEE), the final resolution target of EUV lithography with high-numerical aperture (0.55 NA) scanner is set to sub-10 nm.[5]

Photoresists are light-sensitive materials that undergo a chemical change when exposed to light, permitting them to be selectively removed away or remain during a subsequent developing step. Photoresists play a particularly important role in EUV photolithography. Namely, the energy (92 eV) of EUV light is higher by 14 times than that of a deep ultraviolet (DUV) source (e.g., ArF with 6.4 eV). Considering that the number of photons is inversely proportional to the energy, the EUV scanner generates the probabilistic distribution of photons, which causes a photon shot noise problem and has an adverse effect on critical dimension (CD) and line-edge roughness (LER) of patterns.[6,7]

Figure 1a compares the photoresist characteristics between chemically amplified resist (CAR)-type polymer resists, metal-oxo clusters, and molecular organometallic resists for EUV in the context of the size of the unit particle and the RLS tradeoff relationship, which encompasses sensitivity, resolution, LER, and etch resistance.[8] The traditional CAR-type polymer photoresists require a photoacid catalyst that facilitates the chemical reaction upon photoirradiation. The use of photoacids helps avoid the problem of photon shot noise, enabling effective utilization even at lower doses.[9] However, CAR photoresists have limitations in achieving nanopatterning with EUV lithography.[10−12] Among others, (i) due to the large diameter of free gyration of polymer (around 2−10 nm)[13−16] and (ii) acid diffusion,[17] sub-20 nm patterning with sharp contrast is difficult to achieve. (iii) During the postexposure baking (PEB) step before the developing process, acid diffusion mechanisms are accelerated and cause bridging or pinching failure patterns, thereby increasing LER.[18] (iv) Traditional CAR-type polymer photoresists that are composed

Received: February 11, 2024
Revised: March 15, 2024
Accepted: March 15, 2024
Published: March 27, 2024

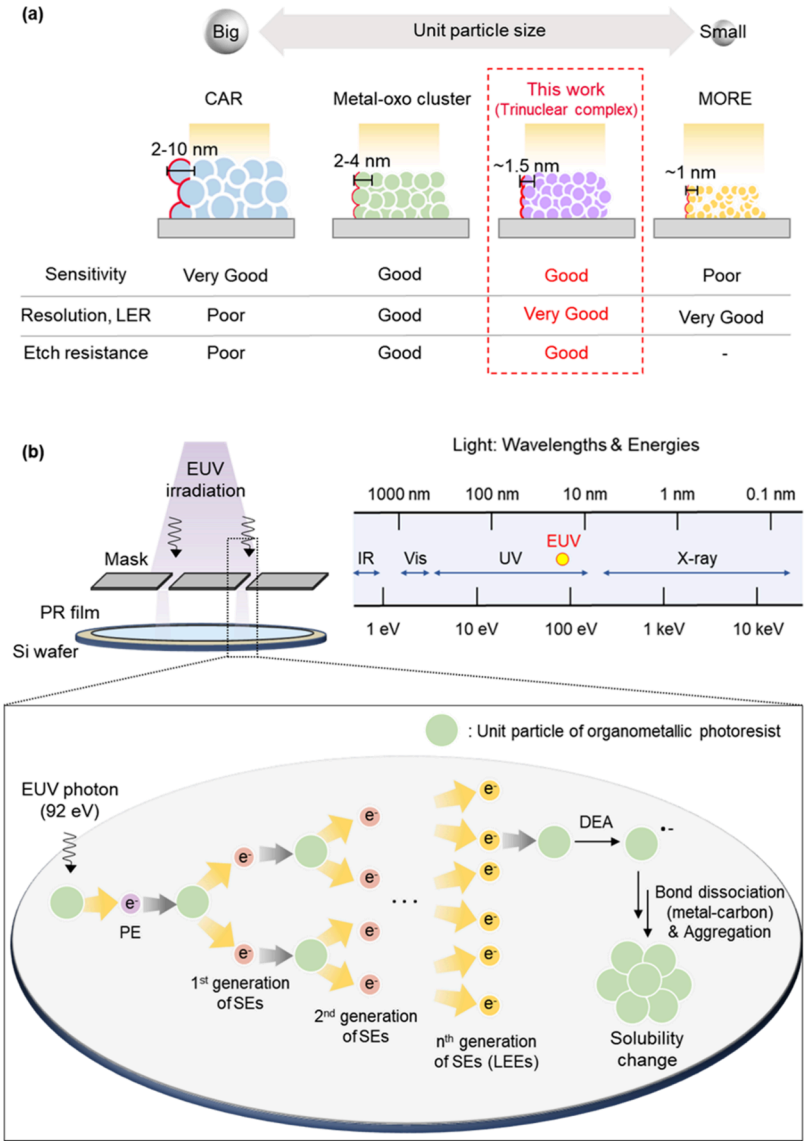

Figure 1. (a) Relationship between the RLS tradeoff and types of wet photoresists. See the texts for detailed explanations (CAR: chemically amplified resist; MORE: molecular organometallic resists for EUV).[8] (b) Proposed mechanism of organometallic photoresists under EUV photon exposure (PE: photoelectron, SE: secondary electron, LEE: low-energy electrons (<20 eV),[23,24] DEA: dissociative electron attachment).

of organic matters exhibit poor etching resistance, thereby making it difficult to produce low-aspect-ratio nanopatterns.[13,15,17,19−22]

To overcome the problems arising from the intrinsic properties of the conventional photoresist materials, metal atoms such as Sn, Hf, Bi, Zn, In, Zr, Cu, and Cr, which exhibit high absorption coefficients over EUV, have been recently incorporated into organic ligands to afford efficient photoresists of small-molecule coordination complexes[25−33] or nanoclusters.[34−43] The size of unit particles in the new materials is smaller and/or more uniform than that of the CAR-type polymer photoresists, making the coordinative materials promising for the next-generation EUV photoresists.[11,44,45] Studies involving organometallic resists in a small-molecule form have depended mostly on single metal centers. Figure 1b depicts the typical EUV-photochemical reaction mechanism of organometallic photoresists containing metal−carbon bonds. Upon irradiation of EUV, the high-energy photons excite the core electrons, ejecting photoelectrons (PE), which subsequently diffuse and interact with the neighboring atoms to produce secondary electrons (SE). These processes continue until low-energy electrons (LEEs) with energies below 20 eV are generated.[23,24,46−49] The LEEs cause a dissociative electron attachment (DEA) reaction, leading to ionization of the photoresist, dissociation of weak bond (usually, Sn−C bond in a tin-based organometallic moiety), and cross-linking between the resulting radical species.[50−52]

Despite stimulating studies that utilize small-molecule metal complexes for efficient EUV photoresists, the best is yet to come. While individual small-molecule metal complexes usually contain one reactive metal center for cross-linking reaction and may require high doses,[25,53] It is hypothesized that multinuclear metal complex photoresists, which are between the small molecules and nanoclusters in size, would undergo multiple cross-linking reactions in a molecule and 3D interconnection with the neighboring molecules. A larger fraction of a multinuclear macrocyclic complex would undergo

https://doi.org/10.1021/acsmaterialsau.4c00010
ACS Mater. Au 2024, 4, 468−478

a cross-linking reaction since there are fewer molecules per volume, due to the large size of the macrocyclic structure with multiple metal centers. Therefore, it is anticipated that multinuclear complex resists may offer improved photosensitivity (i.e., lower doses for the solubility transition).

We herein investigate the photoresist performance of a macrocyclic multinuclear tin complex in EUV lithography. A trinuclear tin complex was synthesized by a one-step reaction between dimethyltin oxide and salicylhydroxamic acid for metal precursor and ligand, respectively. The structure of the resulting complex was characterized with ^{1}H, ^{13}C, and ^{119}Sn NMR spectroscopies, FT-IR spectroscopy, and single-crystal X-ray diffraction; the photochemical reaction of the corresponding film was studied by solid-state NMR and X-ray photoelectron spectroscopies. The thermal, air, and humidity stabilities of the new photoresist were evaluated. Various solvents and postexposure baking (PEB) temperatures were screened for the development conditions. The lithographic performance of the multinuclear complex resist was tested by e-beam and EUV (using microfield exposure tool 5, MET 5, in Lawrence Berkeley National Lab, LBNL) lithography. The EUV experiment revealed that, at a dose of 132.3 mJ/cm^2 and a focus of −20 nm, the observed 20 nm half-pitch (hp) pattern exhibited an LER of 1.1 nm, while the line-width roughness (LWR) was measured at 1.5 nm.

BACKGROUND

Elements such as Sn, Sb, Te, Xe, and Cs and elements with atomic numbers greater than 83 (e.g., At, Fr, Ra, Ac) exhibit high photoabsorption cross-section values at a wavelength of 13.5 nm.[54,55] Among these, Sn stands out as a particularly advantageous choice due to its ease of handling and cost-effectiveness. Sn has high atomic absorption cross-section (1.09×10^7 cm^2/mol) for photons with an energy of 92 eV.[45]

To our knowledge, two studies have thus far presented the potential of multinuclear metal complexes for photoresists in EUV or related photolithography. In 2023, Gonsalves and co-workers[56] have tested the performance of organotin-based cyclotrimeric species for DUV (~254 nm) lithography. They conducted XPS analysis for the 20 nm thick film of the compound before and after DUV exposure and observed the removal of the butyl chain and oxidation of carbon atoms. The oxygen contents increased upon DUV irradiation, attributed to the photochemical formation of the Sn−OH and Sn−O−Sn network. They showed a 10 nm line and 40 nm space patterns with e-beam lithography using the organotin photoresist. In 2022, Ku and co-workers[29] synthesized an organic framework of phthalocyanines, and the resulting pores were subsequently filled with Zn atoms. The framework structure exhibited good chemical stability and photochemical reactivity, thereby enhancing the photosensitivity. While a 100 nm pattern with 200 nm space was successfully demonstrated in E-beam lithography, EUV lithography afforded negative-tone patterns with 40−50 nm feature sizes. However, the weak adhesion of the photoresist to the Si substrate made it difficult to realize straight-line patterns.

MATERIALS AND METHODS

Reagents

All reagents were used as supplied, unless otherwise specified. Salicylhydroxamic acid (SHA, ≥98%) and dimethyltin oxide (≥95%) were purchased from Sigma-Aldrich and TCI, respectively. Organic solvents were purchased from Daejung and Sigma-Aldrich.

Instrumentation

Nuclear magnetic resonance (NMR) spectra were collected using a Bruker biospin ASCEND-500 spectrometer (^{1}H 500 MHz, ^{13}C 126 MHz, and ^{119}Sn 187 MHz). Chemical shifts in the NMR spectra were calibrated with respect to the remaining signals from the non-deuterated solvent (CD_2Cl_2, δ = 5.32 ppm in ^{1}H spectra). FT-IR spectra within the 500 to 4000 cm^{-1} range were acquired using the attenuated total reflectance method with an FTIR spectrometer (IR Affinity-1S, Shimadzu). X-ray photoelectron spectroscopy (XPS) analyses were performed using a Thermo Scientific K-Alpha photoelectron spectrometer with a monochromatic Al Kα source (1486.6 eV) and a He I source. The Casa-XPS software was employed to analyze the peak shapes in the core-level photoelectron spectra, and a linear-type background correction was applied. The obtained XPS spectra were calibrated by using the C 1s peak at 284 eV of adventitious carbon. The high-resolution XPS peaks were deconvoluted by a linear combination function of Lorentzian (30%) and Gaussian (70%). Cross-polarization magic-angle spinning nuclear magnetic resonance (CPMAS-NMR) data were acquired on Bruker 400 MHz AVANCE III HD instrument (^{119}Sn 149 MHz) using a 4 mm Bruker HX-MAS probe at Korea Basic Science Institute (KBSI) western Seoul center. The position of the isotropic signal was verified by performing experiments at a different spinning rate (12 kHz), and the final CPMAS-NMR spectra reported in this paper were obtained at a spinning rate of 14 kHz. Single crystal X-ray diffraction (XRD) data were obtained by using a Bruker CCD diffractometer with SMART and SAINT-plus software (Bruker). The X-ray radiation source used was Mo Kα with a wavelength of 0.71073 Å. Thermogravimetric analysis (TGA) thermogram was obtained by heating from room temperature to 900 °C at a rate of 10 °C/min under air conditions using Ta Instruments (SDT-650). The data for thin film thickness were obtained using a J.A. Woollam (Alpha-SE) ellipsometer. The angles of incidence were measured at 65°, 70°, and 75°. Our ellipsometry analysis was conducted over randomly selected regions. E-beam lithography and surface imaging were performed using a field emission-scanning electron microscope (FE-SEM, JSM 7001F, JEOL) and the Elphy Quantum software program. The EUV tests were conducted using MET 5 at LBNL (CA, USA). The MET 5 lithography system utilized a 13.5 nm synchrotron light source, and the numerical aperture (NA) was 0.55. The critical dimension-scanning electron microscope (CD-SEM, S-9260A, Hitachi) was used to measure the LWR of patterns; 32 randomly chosen points were analyzed.

RESULTS AND DISCUSSION

Synthesis

A trinuclear tin complex (denoted as TTC) was synthesized by modifying the previous method,[57] in one step, using dimethyltin oxide and salicylhydroxamic acid (SHA) (Scheme 1). See the Supporting Information for detailed experimental procedures. Our macrocyclic resist was designed to have no

Scheme 1. Synthetic Scheme for the Trinuclear Macrocyclic Tin Complex (TTC) from Dimethyltin Oxide and Salicylhydroxamic Acid (SHA)

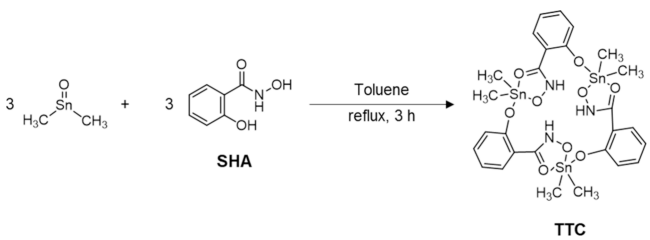

https://doi.org/10.1021/acsmaterialsau.4c00010
ACS Mater. Au 2024, 4, 468−478

Sn−OH group to improve the resistance to atmospheric moisture while addressing the RLS tradeoff.[58] In metal-oxo cluster photoresists, the presence of metal-OH groups can potentially result in condensation reactions during the heating process, such as soft baking at temperatures around 70 °C.[59−61]

Characterization

We characterized the multinuclear complex with powder FT-IR spectroscopy (Figure 2a). The free ligand (SHA) exhibited

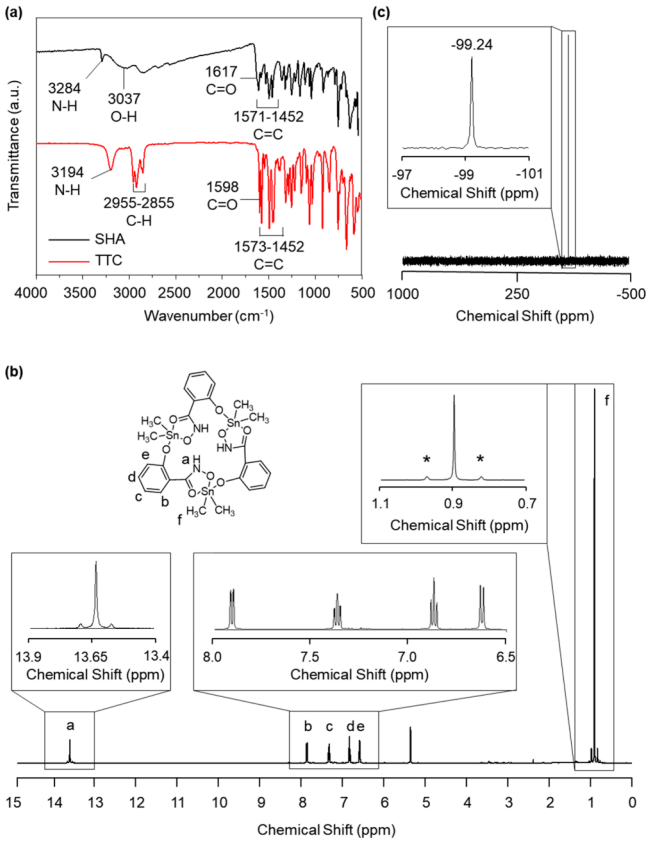

Figure 2. (a) FT-IR spectra of salicylhydroxamic acid (SHA) and TTC powder. (b) ^{1}H NMR spectrum of the TTC. Insets show splitting patterns and satellite peaks (*). (c) ^{119}Sn NMR spectrum of the TTC. Inset shows the singlet pattern.

a broad band at around 3037 cm^{-1} and multiple peaks at around 1617 cm^{-1}, indicative of the presence of the −OH group and hydrogen bonding of the carbonyl group,[62,63] respectively. After the reaction with the Sn precursor, the following changes were observed. (i) The broad band of the −OH group disappeared. (ii) A new peak corresponding to the C−H stretching vibration emerged in the range of 2955−2855 cm^{-1}.[64−67] (iii) The carbonyl stretch peak was shifted slightly to a lower frequency (1598 cm^{-1}).[66,67]

Figure 2b shows the ^{1}H NMR spectrum of the macrocyclic complex (refer to Figures S1−S3 for the full spectra). The proton resonance at 10.53 ppm corresponding to N−H of the free ligand disappeared after the reaction while a new deshielding peak at 13 ppm appeared.[68] The methyl protons were identified with the single peak at 0.85 ppm, and satellite peaks arising from the interaction with the adjacent Sn atom were observed with $^{2}J_{Sn-H}$ of 80 Hz. The Lockhart and Manders equation (eq 1) suggests that the coupling constant ($^{2}J_{Sn-H}$) between Sn(IV) and methyl group could be used to estimate the C−Sn−C bonding angle (θ(C−Sn−C)):[69]

$$\theta(\mathrm{C-Sn-C}) = 0.0161(^{2}J_{\mathrm{Sn-H}})^{2} - 1.32(^{2}J_{\mathrm{Sn-H}}) + 133.4 \quad (1)$$

According to eq 1, the θ(C−Sn−C) value in our macrocyclic tin complex was revealed to be 130.8°, which implies a five-coordinated tin complex. The chemical shift of ^{119}Sn NMR peak, −99.24 ppm (Figure 2c), fell within the range reported for five-coordination tin compounds.[70] These results are consistent with the data obtained from single crystal X-ray diffraction (XRD) (see below for details).

Single-Crystal XRD Study

The solid-state structure of TTC was analyzed with a single-crystal X-ray diffraction study. See Table S1 for the detailed result. As shown in Figure 3, TTC consisted of three Sn atoms

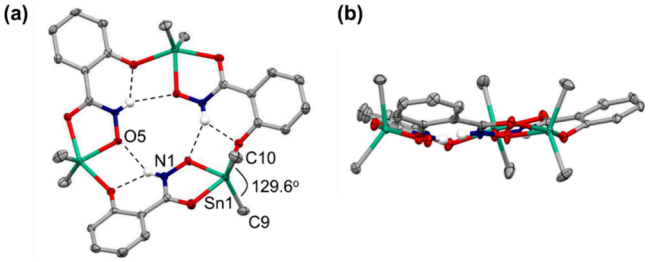

Figure 3. (a) Top and (b) side views of the X-ray crystal structure of TTC. For the sake of clarity, hydrogen atoms and solvent molecules were excluded, except hydrogens on the nitrogen atoms. The labeling and coloring schemes are as follows: green, dark blue, red, and gray for Sn, N, O, and C atoms, respectively.

and three deprotonated SHA ligands, indicative of successful synthesis of the desired macrocyclic structure. Three Sn atoms displayed a five-coordinate structure with a distorted trigonal-bipyramidal geometry. The Sn(1)−C(9) bond distance was measured to be 2.110 Å; the bonding angle of C(9)−Sn(1)−C(10) was 129.6°, consistent with the one (130.8°) determined by ^{1}H NMR analysis. The N(1)−O(5) bond distance was 3.1 Å, falling within the typical range indicative of N−H···O hydrogen bonding.[71] The intramolecular hydrogen bonding seems to enhance the stability of macrocyclic structure.[72] The other two Sn-SHA coordination moieties also exhibited a similar structure.

Spin-Coating and Develop Process

The multinuclear complex was dissolved in toluene (2 wt%). The resulting solution was filtered through a PTFE syringe filter (0.2 μm) and spin-coated onto a 4 in. Si wafer at a speed of 3000 rpm for 30 s. The coated wafer was prebaked at 130 °C for 90 s to remove residual solvent. According to ellipsometry analysis, the thickness of our resist film was 44 nm with good uniformity. The uniformity was further confirmed by AFM analysis, which revealed a root-mean-square (RMS) roughness of 0.407 nm. The spin-coated wafer was partially exposed to ∼254 nm UV light (4 W) for 3 h in air and subsequently subjected to postexposure bake (PEB) at 180 °C for 90 s. The partially exposed photoresist film was developed by immersing it in various solvents for 30 s. Figure S4 depicts each of the steps, and Table S2 summarizes the solvent test result. We chose PGMEA (propylene glycol monomethyl ether acetate) as the developer for our photo-

https://doi.org/10.1021/acsmaterialsau.4c00010
ACS Mater. Au 2024, 4, 468−478

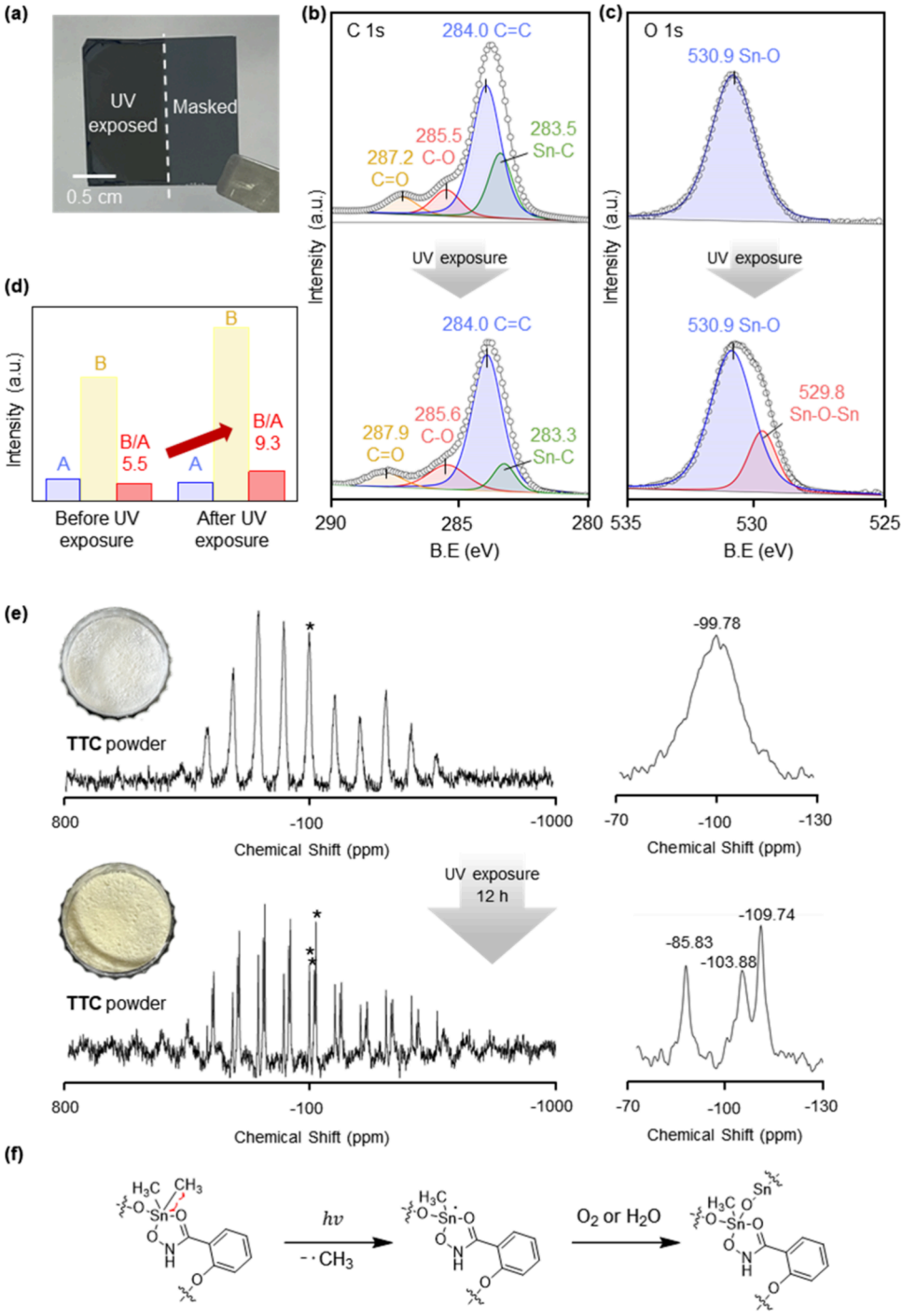

Figure 4. (a) Photograph of TTC photoresist film after partial UV-exposure and development with PGMEA. The masked area was dissolved efficiently by the developer. (b, c) High-resolution XPS spectra of C 1s and O 1s for TTC photoresist films before and after UV exposure. (d) Comparison of the change in ratio of C 1s peak corresponding to Sn−C and C═C and Sn 3d peak, before and after UV exposure. "A" represents the area of the blue (Sn−C or C═C) peak in the C 1s XPS spectra, while "B" represents the total area of the Sn 3d peaks in the XPS spectra (Figure S5 in the Supporting Information). (e) Photographs of TTC powder before and after UV exposure, and the corresponding ^{119}Sn CPMAS-NMR spectra. Isotropic peaks are indicated by asterisks, and these isotropic peaks are magnified on the right side of each corresponding full spectrum. (f) The proposed photochemical reaction mechanism of TTC under ambient conditions.

resist. Figure 4a shows a photograph of the final film after the development. As a negative photoresist, the unexposed area was dissolved efficiently by the PGMEA developer while the UV-exposed area remained. Ellipsometry analysis revealed that the thickness of the film that was exposed and not exposed to the UV light was 29.5 and 1.9 nm, respectively.

Solid-State Analysis of the Multinuclear Complex Resist Film

We analyzed the film with X-ray photoelectron spectroscopy (XPS) before and after UV irradiation. In the C 1s spectra (Figure 4b), four components were observed at 283.5, 284.0, 285.5, and 287.2 eV, corresponding to Sn−C, C═C, or adventitious carbon, C−O, and C═O. The O 1s spectrum of

https://doi.org/10.1021/acsmaterialsau.4c00010
ACS Mater. Au 2024, 4, 468−478

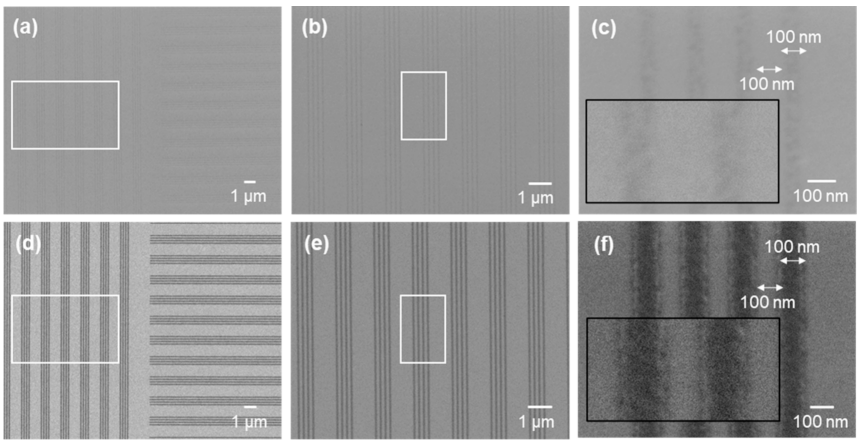

Figure 5. FE-SEM images of 200 nm L/S patterns created using a 44 nm-thick TTC based photoresist film in e-beam lithography (1500 $\mu C/cm^2$ dose and 10 nm step size with 30 keV e-beam). Panels (a−c) and (d−f) illustrate the patterns developed without and with the 180 °C PEB process, respectively. Panels (b, e) are × 2 zoom-in view of the white rectangular regions in panels (a, d), respectively, while panels (c, f) present × 10 zoom-in of the white rectangular regions in the panels (b, e).

the pristine film exhibited a dominant peak at 530.9 eV, which was assigned to the Sn−O bond (Figure 4c).[73] After UV irradiation, the new peak at 529.8 eV, corresponding to the Sn−O−Sn bond appeared. The peak at 533.4 eV corresponding to the residual Sn−OH potentially induced by adsorption of airborne adventitious water molecules,[74,75] was not detected, indicating good resistance of TTC over humidity. The peak at 529.8 eV corresponding to the Sn−O−Sn linkage appeared in the O 1s spectrum after irradiation, indicating the occurrence of a Sn−O−Sn network under UV exposure. Figure 4d shows that the ratio of the total area of the Sn 3d peak to the blue peak (Sn−C or C═C) area of C 1s increased from 5.5 to 9.3 after UV exposure of the TTC photoresist film. This increased ratio was attributed to the dissociation of $Sn-CH_3$ and loss of the methyl substituents, presumably generating Sn radical species and cross-linking between them to produce Sn−O−Sn bonds (further supported by the new peak appearance in the O 1s XPS spectrum of Figure 4c). The Sn 3d spectrum showcased a spin−orbit doublet with Sn 3d5/2 at 486.2 eV and Sn 3d3/2 at 494.6 eV, presenting a difference of 8.4 eV (Figure S5). These values suggest the + 4 oxidation state of Sn atoms.[76] No discernible alterations were observed in the Sn 3d spectra before and after UV irradiation, indicating no significant change in the oxidation states of the Sn atoms. We also conducted FT-IR spectroscopic analysis over our resist before and after UV exposure and found that the peak intensity of the C−H bond was significantly reduced while the other peaks remained nearly unchanged. In combination with the XPS data of Figure 4b, we could assume that the methyl group connected to the tin atom disappeared by the UV irradiation.

The solid-state photochemical reaction of TTC was further characterized by solid-state NMR spectroscopy. Upon UV irradiation, the color of TTC power changed from white to light yellow (Figure 4e). The UV-exposed TTC powder was insoluble in both water and organic solvents. We also observed significant changes in ^{119}Sn CPMAS-NMR (cross-polarization magic-angle spinning NMR) spectra (see Figures S6 and S7 for the full spectra). The pristine TTC power exhibited a single peak at −99.78 ppm, which concurs with the chemical shift of the solution NMR (−99.24 ppm in CD_2Cl_2). After exposure to the UV light, three distinct peaks at −85.83, −103.88, and −109.74 ppm were observed, indicating considerable change in the coordination environment of Sn. Considering that the chemical shift of ^{119}Sn within the ranges of −210 to −400, −90 to −190, and 200 to −95 ppm is indicative of six-, five-, and four-coordinated Sn atoms, respectively,[69,70,77,78] the peak at −85.83 ppm corresponds to the newly produced four-coordinated Sn complex, while the coexistence of two distinct five-coordinated Sn complexes is revealed by the other peaks at −103.88 and −109.74 ppm. All the XPS and CPMAS-NMR data and the observation of solubility change indicate the photochemical activity of TTC and the occurrence of solid-state cross-linking reaction by UV. Figure 4f shows the proposed mechanism of the photochemical reaction of TTC under ambient conditions.[73]

E-Beam Lithography

We tested the patterning ability of our multinuclear complex resist using e-beam lithography for the pre-evaluation of EUV lithography.[79] The 44 nm-thick film of TTC on the Si wafer was patterned using a 30 keV e-beam with a dose range from 95 to 1500 $\mu C/cm^2$ and a 10 nm step size, followed by development with PGMEA for 30 s to produce a 200 nm L/S (100 nm line and 100 nm space) pattern. The minimal dose that was sufficient for producing the desired L/S patterning was 665 $\mu C/cm^2$. Figure 5a−c shows SEM images obtained with FE-SEM at the dose of 1500 $\mu C/cm^2$. The pattern was blurry, and the line-edge roughness (LER) of the pattern was considerable as shown in Figure 5c, which could be due to back-scattered electrons. To examine the effect of PEB, we compared the pattern with an analogous one exposed to the PEB at 180 °C for 90 s and developed with PGMEA. As shown in Figure 5d−f, we observed enhanced contrasts and small LER compared to the pattern developed without PEB, which indicates the importance of PEB in improving the resolution of the lithographic pattern.

EUV Experiment and CD-SEM Analysis

We further probed the performance of our macrocylic tin complex by EUV lithography. The 44 nm-thick film was prepared on 8 in. notch-type Si wafer. The EUV exposure was performed using MET 5 from Lawrence Berkeley National Laboratory (LBNL). The exposure focus bias was 20 nm, and the dose was increased exponentially from 49.7 to 201.1 mJ/cm^2. A mask (IMO410298) provided by the LBNL was used to form L/S patterns with various feature sizes. The PEB

https://doi.org/10.1021/acsmaterialsau.4c00010
ACS Mater. Au 2024, 4, 468−478

condition was set to 130 °C for 90 s or 180 °C for 90 s. After the EUV exposure, PGEMA was used as the developer for 30 s, and hard baking at 150 °C for 5 min was carried out. The ADI (after development inspection) with critical dimension-scanning electron microscopy (CD-SEM) was used to determine CD, LER, and line-width roughness (LWR) of patterns. We found that the PEB condition was critical for determining the minimum dose for patterning: the patterns produced by PEB at 180 °C were much clearer than those by PEB at 130 °C. The best shot was observed in the condition: dose of 132.3 mJ/cm^2, focus of −20 nm, and focus margin from 0 to −40 nm.

Figure 6a–d presents CD-SEM images of the patterns formed at various sizes under the conditions, with the insets

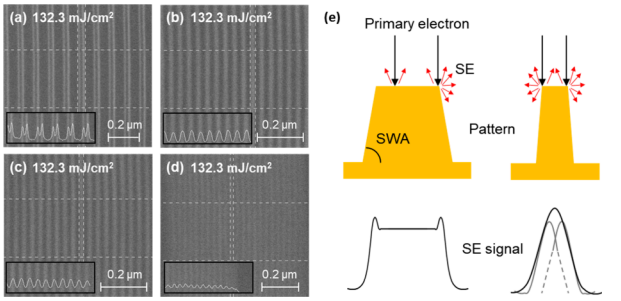

Figure 6. ADI CD-SEM images of (a) 50P100, (b) 20P40, (c) 18P36, and (d) 16P32 L/S patterns obtained from EUV lithography of TTC film in the dose of 132.3 mJ/cm^2. Insets show secondary electron (SE) signals. (e) Schematic illustrating SE signals resulting from the interaction between patterns and primary electrons in CD-SEM.[96,97] (SWA: sidewall angle).

showing the secondary electron (SE) signals. Figure 6a depicts L/S patterns corresponding to 50P100 (design CD = 50 and 100 nm pitch). The two intensive SE peaks were observed, attributable to the edges of the trapezoidal pattern. The trapezoidal structure probably resulted from the Fresnel diffraction that occurs when light passes through a slit.[75,76] As the pattern size decreased, only one round-shaped SE signal was observed (Figure 6b–d). The CD-SEM analysis indicated that the LER ranged from 1.1 to 1.9 nm. Particularly, the smallest 20P40 pattern showed 1.1 nm LER, which is quite low compared to the literature values.[80−92] The LWR in the 20P40 pattern was determined to be 1.5 nm (the average value of LWR was obtained from Figure S11 of SI), which is comparable to or better than the values reported in the literature.[93−95] We observed a nonclear L/S pattern in the 16P32 region (design CD = 16 nm, 32 nm pitch) (Figure 6c). The possible reason would be that, as depicted in the right panel of Figure 6e, as the CD decreases, the edge peaks can merge, resulting in a round shape.

Figure 7 presents a diagram summarizing the results of EUV tests for previously reported PRs and TTC, in terms of LER, half-pitch (HP), and sensitivity.[80−92] The performance of the photoresist could be gauged with the *Z*-factor, which is calculated with eq 2:[98]

$$Z - \text{factor} = [\text{Resolution}]^3 \times [\text{LER}]^2 \times [\text{Sensitivity}]^1 \quad (2)$$

The *Z*-factor is a metric used to evaluate the performance of photoresists by considering the RLS tradeoff.[79] The calculated *Z*-factor value for our macrocyclic photoresist was 1.28 × 10^{-8}

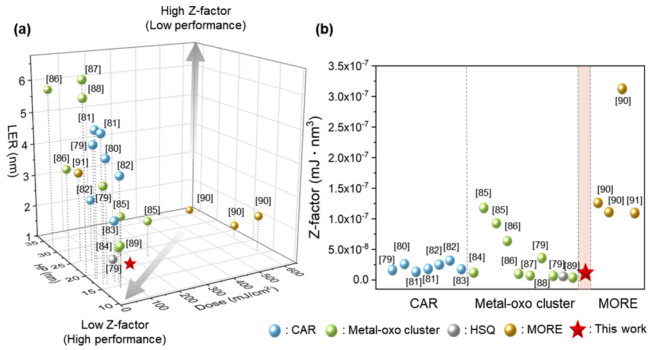

Figure 7. (a) Comparison of EUV photoresist performance between our TTC and literature studies that have reported sub-30 nm feature sizes, in terms of half-pitch (HP, nm), dose (mJ/cm^2), and line edge roughness (LER, nm). The gray arrows correlate the three factors with photoresist performance and *Z*-factor (see eq 2 in the main texts). (b) Plot of the *Z*-factor of the photoresists reported in the literature and our one. We categorized the photoresists according to the size of the unit particle. Table S3 in the Supporting Information summarizes the data.[80−92] The numbers in parentheses are the references cited herein.

mJ·nm^3, indicating good performance compared to the reported photoresist materials (Figure 7). Generally, an aspect ratio of below 2:1 is recommended for photolithographic patterning. In this regard, we assume that our film was rather thick (44 nm), and the 16P32 pattern has a bit higher aspect ratio (2.8:1) than the ideal one. Hence, we anticipate that decreasing the film thickness and minimizing the processing time would lead to patterns of higher quality. TTC exhibited noticeably low LER (1.1 nm), being comparable with that of HSQ (hydrogen silsesquioxane, ∼1.5 nm).[80] When compared to the performances of the existing MORE in the literature, our macrocyclic photoresist showed good resolution: the LER was reduced by 21.4% in the 10% smaller line features, and the sensitivity was improved by over 4.5 times.[91] It is noteworthy that given that the performance of photoresist can rely on not only intrinsic properties of photoresist chemicals but also specifications of EUV scanner equipment, the great performance of TTC might be due to any differences in photolithographic conditions across the studies (see Table S3 for the differences). Further studies are required to clarify this issue.

Stability

The stability of a photoresist is an important issue for industrial applications. For example, the good-performing photoresist of HSQ has shown poor storage stability (5 °C storage, 6 months), hindering its practical application.[99,100] To test the storage stability, we left the TTC photoresist solution in the air at room temperature for over 6 months, without light shielding. ^{1}H NMR spectroscopic analysis indicates no change in the ^{1}H NMR spectrum (Figure S8), indicating good storage stability. Furthermore, the TTC powder exhibited great humidity stability. As shown in Figure S9 in the Supporting Information, after exposure of TTC to deionized water and sonication for 2 min, no significant change in the ^{1}H NMR spectrum was observed. We also examined the thermal stability of our multinuclear complex photoresist by conducting thermogravimetric analysis (TGA) in the temperature range from room temperature to 900 °C. The multinuclear complex started to decompose at 218 °C, and the temperature of 5 weight loss percentage (wt%) was about 223 °C (Figure S10). Beyond 535 °C, a constant weight of ∼48.4% was maintained,

https://doi.org/10.1021/acsmaterialsau.4c00010
ACS Mater. Au 2024, 4, 468−478

which would be indicative of full oxidation of TTC to SnO_2. In addition, to determine the appropriate PEB temperature range, whether the TTC photoresist undergoes thermal-induced cross-linking without light irradiation was examined by baking the spin-coating TTC film on a hot chuck at various temperatures (from 130 to 210 °C). After baking, each spin-coated TTC sample was partially immersed in PGMEA. We found that cross-linking reactions are not initiated in the tested temperature range, which indicates selective cross-linking in the photochemical conditions, and not in the thermal conditions, verifying the suitability of our PEB condition in the development process (Figure S10). The thermal property of TTC signifies that the multinuclear tin complex photoresist can maintain its stability and functionality even during semiconductor manufacturing processes conducted at high temperatures, such as PEB (typically 70−150 °C) and other related steps.

CONCLUSION

In this study, we synthesized a new macrocyclic multinuclear tin complex and evaluated its photoresist performance. The structure was confirmed in solution and solid states using NMR, FT-IR, and single-crystal XRD. The photolytic reaction of the new resist was probed with XPS and solid-state NMR analyses. The photolithographic feature of the resist was evaluated by a simple UV lamp in the lab, e-beam lithography, and an EUV scanner in the synchrotron. In the EUV test utilizing MET 5, we achieved successful nanopatterning with a small *Z*-factor (1.28×10^{-8} mJ·nm^3). The remarkably good thermal, air, and humidity stabilities of the new resist make it promising for practical application. The results presented herein suggest that multinuclear complex photoresists can be a new class of resists in the semiconductor industry utilizing EUV photolithography.

ASSOCIATED CONTENT

Data Availability Statement

The supplementary crystallographic data for this paper can be found in CCDC 2300842 and is available at no cost through www.ccdc.cam.ac.uk/data_request/cif.

Supporting Information

The Supporting Information is available free of charge at https://pubs.acs.org/doi/10.1021/acsmaterialsau.4c00010.

Experimental details for synthesis and characterization of TTC, and photolithography process; ^{1}H, ^{13}C, and ^{119}Sn NMR, ^{119}Sn CPMAS-NMR, FTIR, and XPS spectra; TGA data; AFM topography data; CD-SEM images; X-ray single-crystal diffraction data; developing test results of TTC film; and summary of HP, LER, dose, and calculated *Z*-factor values reported in the literature (PDF)

AUTHOR INFORMATION

Corresponding Author

Hyo Jae Yoon − *Department of Chemistry, Korea University, Seoul 02841, Republic of Korea;* orcid.org/0000-0002-2501-0251; Email: hyoon@korea.ac.kr

Authors

Gayoung Lim − *Department of Chemistry, Korea University, Seoul 02841, Republic of Korea*

Kangsik Lee − *Department of Chemistry, Korea University, Seoul 02841, Republic of Korea*

Chawon Koh − *Semiconductor R&D Center, Samsung Electronics Co., Ltd, Gyeonggi-do 18448, Republic of Korea; Department of Materials Science and Engineering, Yonsei University, Seoul 03722, Republic of Korea*

Tsunehiro Nishi − *Semiconductor R&D Center, Samsung Electronics Co., Ltd, Gyeonggi-do 18448, Republic of Korea*

Complete contact information is available at: https://pubs.acs.org/10.1021/acsmaterialsau.4c00010

Author Contributions

[‖]G.L. and K.L. contributed equally to this work. CRediT: **Gayoung Lim** data curation, formal analysis, investigation, visualization, writing-original draft, writing-review & editing; **Kangsik Lee** data curation, formal analysis, investigation, writing-review & editing; **Chawon Koh** formal analysis, investigation, writing-review & editing; **Tsunehiro Nishi** investigation, methodology, writing-review & editing; **Hyo Jae Yoon** conceptualization, funding acquisition, investigation, project administration, supervision, writing-original draft, writing-review & editing.

Notes

The authors declare no competing financial interest.

ACKNOWLEDGMENTS

This research was supported by Samsung Electronics and the NRF of Korea (NRF-2019R1A6A1A11044070). We are grateful to S. Hong and C. S. Hong for X-ray crystallographic analysis, and H. S. Jeong for e-beam lithography. Korea advanced nano fab center (KANC) kindly provided the equipment and facilities for CD-SEM analysis.

REFERENCES

(1) Miyazaki, J.; Yen, A. EUV lithography technology for high-volume production of semiconductor devices. *J. Photopolym. Sci. Technol.* **2019**, *32* (2), 195−201.

(2) Fay, B. Advanced optical lithography development, from UV to EUV. *Microelectron. Eng.* **2002**, *61*−*62*, 11−24.

(3) Hasan, R. M. M.; Luo, X. Promising lithography techniques for next-generation logic devices. *Nanomanuf. Metrol.* **2018**, *1* (2), 67−81.

(4) van Schoot, J.; van Setten, E.; Rispens, G.; Troost, K.; Kneer, B.; Migura, S.; Neumann, J. T.; Kaiser, W. High-numerical aperture extreme ultraviolet scanner for 8-nm lithography and beyond. *J. Micro/Nanolithogr., MEMS, MOEMS* **2017**, *16* (4), No. 041010.

(5) Van Schoot, J. The Moore's law machine: the next trick to tinier transistors is high-numerical-aperture EUV lithography. *IEEE Spectrum* **2023**, *60* (9), 44−48.

(6) Kruit, P.; Steenbrink, S. Local critical dimension variation from shot-noise related line edge roughness. *J. Vac. Sci. Technol. B* **2005**, *23* (6), 3033−3036.

(7) Kruit, P.; Steenbrink, S.; Wieland, M. Predicted effect of shot noise on contact hole dimension in e-beam lithography. *J. Vac. Sci. Technol. B* **2006**, *24* (6), 2931−2935.

(8) Cardineau, B. Chapter 11 - Molecular organometallic resists for EUV (MORE). *Front. Nanosci.* **2016**, *11*, 377−420.

(9) Yoshizawa, M.; Moriya, S. Study of the acid-diffusion effect on line edge roughness using the edge roughness evaluation method. *J. Vac. Sci. Technol. B* **2002**, *20* (4), 1342−1347.

(10) Suzuki, M.; Kim, Y.; Her, Y.; Wu, H.; Si, K.; Maturi, M. M.; Fackler, P. H.; Moinpour, M.; Dammel, R.; Cao, Y. Negative-tone resists for EUV lithography. *Proc. SPIE* **2023**, *12498*, No. 1249813.

(11) Ghosh, S.; Pradeep, C. P.; Sharma, S. K.; Reddy, P. G.; Pal, S. P.; Gonsalves, K. E. Recent advances in non-chemically amplified

photoresists for next generation IC technology. *RSC Adv.* **2016**, *6* (78), 74462−74481.
(12) Lim, G.; Lee, K.; Choi, S.; Yoon, H. J. Organometallic and coordinative photoresist materials for EUV lithography and related photolytic mechanisms. *Coord. Chem. Rev.* **2023**, *493*, No. 215307.
(13) Patsis, G. P.; Nijkerk, M.D.; Leunissen, L.H.A.; Gogolides, E. Simulation of material and processing effects on photoresist line-edge roughness. *Int. J. Comput. Sci. Eng.* **2006**, *2* (3−4), 134−143.
(14) Sanders, D. P.; Cheng, J.; Rettner, C. T.; Hinsberg, W. D.; Kim, H.-C.; Trung, H.; Fritz, A.; Harrer, S.; Holmes, S.; Colburn, M. Integration of directed self-assembly with 193 nm lithography. *J. Photopolym. Sci. Technol.* **2010**, *23* (1), 11−18.
(15) Ober, C. K.; Xu, H.; Kosma, V.; Sakai, K.; Giannelis, E. P. EUV photolithography: resist progress and challenges. *Proc. SPIE* **2018**, *10583*, No. 1058306.
(16) Otsubo, Y.; Sakai, K.; Kasahara, K.; Xu, H.; Giannelis, E. P.; Ober, C. K. Progress in EUV Photoresists for High-Resolution Patterning. *J. Photopolym. Sci. Technol.* **2022**, *35* (1), 101−104.
(17) Tarutani, S.; Tamaoki, H.; Tsubaki, H.; Takahashi, T.; Takizawa, H.; Takahashi, H.; Kang, S.-J. Characterizing polymer bound PAG type EUV resist. *J. Photopolym. Sci. Technol.* **2011**, *24* (2), 185−191.
(18) Tseng, Y.-F.; Liao, P.-C.; Chen, P.-H.; Gau, T.-S.; Lin, B.-J.; Chiu, P.-W.; Liu, J.-H. Highly hydroxylated hafnium clusters are accessible to high resolution EUV photoresists under small energy doses. *Nanoscale Adv.* **2024**, *6* (1), 197−208.
(19) Levinson, H.; Brunner, T. Current challenges and opportunities for EUV lithography. *Proc. SPIE* **2018**, *10809*, No. 1080903.
(20) Lawson, R.; Lee, C.-T.; Yueh, W.; Tolbert, L.; Henderson, C. Single molecule chemically amplified resists based on ionic and non-ionic PAGs. *Proc. SPIE* **2008**, *6923*, No. 69230K.
(21) Lee, C.-T.; Wang, M.; Jarnagin, N.; Gonsalves, K.; Roberts, J.; Yueh, W.; Henderson, C. Photosensitivity and line-edge roughness of novel polymer-bound PAG photoresists. *Proc. SPIE* **2007**, *6519*, No. 65191E.
(22) Koh, C.; Georger, J.; Ren, L.; Huang, G.; Goodwin, F.; Wurm, S.; Ashworth, D.; Montgomery, W.; Pierson, B.; Park, J.-O; et al. Characterization of promising resist platforms for sub-30-nm HP manufacturability and EUV CAR extendibility study. *Proc. SPIE* **2010**, *7636*, No. 763604.
(23) Ingólfsson, O. *Low-energy electrons: fundamentals and applications*; Pan Stanford Publishing Pte. Ltd., 2019.
(24) Ogletree, D. F. Chapter 2 - Molecular excitation and relaxation of extreme ultraviolet lithography photoresists. *Front. Nanosci.* **2016**, *11*, 91−113.
(25) Del Re, R.; Sortland, M.; Pasarelli, J.; Cardineau, B.; Ekinci, Y.; Vockenhuber, M.; Neisser, M.; Freedman, D.; Brainard, R. Low-LER tin carboxylate photoresists using EUV. *Proc. SPIE* **2015**, *9422*, No. 942221.
(26) Passarelli, J.; Murphy, M.; Del Re, R.; Sortland, M.; Hotalen, J.; Dousharm, L.; Fallica, R.; Ekinci, Y.; Neisser, M.; Freedman, D.; et al. Organometallic carboxylate resists for extreme ultraviolet with high sensitivity. *J. Micro/Nanolithogr., MEMS, MOEMS* **2015**, *14* (4), No. 043503.
(27) Sortland, M.; Hotalen, J.; Del Re, R.; Passarelli, J.; Murphy, M.; Kulmala, T.; Ekinci, Y.; Neisser, M.; Freedman, D.; Brainard, R. Platinum and palladium oxalates: positive-tone extreme ultraviolet resists. *J. Micro/Nanolithogr., MEMS, MOEMS* **2015**, *14* (4), No. 043511.
(28) Passarelli, J.; Cardineau, B.; Del Re, R.; Sortland, M.; Vockenhuber, M.; Ekinci, Y.; Sarma, C.; Neisser, M.; Freedman, D.; Brainard, R. EUV resists comprised of main group organometallic oligomeric materials. *Proc. SPIE* **2014**, *9051*, No. 90512A.
(29) Ku, Y.; Kim, J.-I.; Oh, H.-T.; Kim, Y.; Choi, M.; Lee, J.-K.; Kim, K.-H.; Park, B.-G.; Lee, S.; Koh, C.; et al. Perfluoroalkylated metallophthalocyanines as EUV resist candidates. *Proc. SPIE* **2022**, *12055*, No. 120550D.
(30) Saifullah, M. S.; Asbahi, M.; Binti-Kamran Kiyani, M.; Tripathy, S.; Ong, E. A.; Ibn Saifullah, A.; Tan, H. R.; Dutta, T.; Ganesan, R.; Valiyaveettil, S. Direct patterning of zinc sulfide on a sub-10 nanometer scale via electron beam lithography. *ACS Nano* **2017**, *11* (10), 9920−9929.
(31) Saifullah, M. S.; Asbahi, M.; Neo, D. C.; Mahfoud, Z.; Tan, H. R.; Ha, S. T.; Dwivedi, N.; Dutta, T.; Bin Dolmanan, S.; Aabdin, Z Patterning at the resolution limit of commercial electron beam lithography. *Nano Lett.* **2022**, *22* (18), 7432−7440.
(32) Nandi, S.; Khillare, L.; Moinuddin, M. G.; Kumar, S.; Chauhan, M.; Sharma, S. K.; Ghosh, S.; Gonsalves, K. E. Macrocycle Network-Aided Nanopatterning of Inorganic Resists on Silicon. *ACS Appl. Nano Mater.* **2022**, *5* (8), 10268−10279.
(33) Yogesh, M.; Moinuddin, M. G.; Khillare, L. D.; Chinthalapalli, S.; Sharma, S. K.; Ghosh, S.; Gonsalves, K. E. Organotin bearing polymeric resists for electron beam lithography. *Microelectron. Eng.* **2022**, *260*, No. 111795.
(34) Stowers, J.; Keszler, D. A. High resolution, high sensitivity inorganic resists. *Microelectron. Eng.* **2009**, *86* (4−6), 730−733.
(35) Olynick, D.; Schwartzberg, A.; Keszler, D. A. Chapter 10 - Mainstreaming inorganic metal-oxide resists for high-resolution lithography. *Front. Nanosci.* **2016**, *11*, 349−375.
(36) Frederick, R. T.; Saha, S.; Trey Diulus, J.; Luo, F.; Amador, J. M.; Li, M.; Park, D.-H.; Garfunkel, E. L.; Keszler, D. A.; Herman, G. S. Thermal and radiation chemistry of butyltin oxo hydroxo: A model inorganic photoresist. *Microelectron. Eng.* **2019**, *205*, 26−31.
(37) Kenane, N.; Keszler, D. A. High-resolution lithographic patterning with organotin films: role of CO_2 in differential dissolution rates. *ACS Appl. Mater. Interfaces.* **2021**, *13* (16), 18974−18983.
(38) Grenville, A.; Anderson, J.; Clark, B.; De Schepper, P.; Edson, J.; Greer, M.; Jiang, K.; Kocsis, M.; Meyers, S.; Stowers, J.; et al. Integrated fab process for metal oxide EUV photoresist. *Proc. SPIE* **2015**, *9425*, No. 94250S.
(39) Stowers, J.; Anderson, J.; Cardineau, B.; Clark, B.; De Schepper, P.; Edson, J.; Greer, M.; Jiang, K.; Kocsis, M.; Meyers, S.; et al. Metal oxide EUV photoresist performance for N7 relevant patterns and processes. *Proc. SPIE* **2016**, *9779*, No. 977904.
(40) Cardineau, B.; Del Re, R.; Marnell, M.; Al-Mashat, H.; Vockenhuber, M.; Ekinci, Y.; Sarma, C.; Freedman, D. A.; Brainard, R. L. Photolithographic properties of tin-oxo clusters using extreme ultraviolet light (13.5nm). *Microelectron. Eng.* **2014**, *127*, 44−50.
(41) Li, L.; Chakrabarty, S.; Jiang, J.; Zhang, B.; Ober, C.; Giannelis, E. P. Solubility studies of inorganic−organic hybrid nanoparticle photoresists with different surface functional groups. *Nanoscale* **2016**, *8* (3), 1338−1343.
(42) Namatsu, H.; Takahashi, Y.; Yamazaki, K.; Yamaguchi, T.; Nagase, M.; Kurihara, K. Three-dimensional siloxane resist for the formation of nanopatterns with minimum linewidth fluctuations. *J. Vac. Sci.* **1998**, *16* (1), 69−76.
(43) Liu, F.-F.; Wang, D.; Chen, G.-H.; Qiao, Y.; Luo, F.; Zhang, J.; Zhang, L. Alkenyl-type ligands functionalized tin-lanthanide oxo nanoclusters as molecular lithography resists. *Sci. China Chem.* **2023**, *66*, 1731−1736.
(44) Luo, C.; Xu, C.; Lv, L.; Li, H.; Huang, X.; Liu, W. Review of recent advances in inorganic photoresists. *RSC Adv.* **2020**, *10* (14), 8385−8395.
(45) Ouyang, C. Y.; Chung, Y. S.; Li, L.; Neisser, M.; Cho, K.; Giannelis, E. P.; Ober, C. K. Non-aqueous negative-tone development of inorganic metal oxide nanoparticle photoresists for next generation lithography. *Proc. SPIE* **2013**, *8682*, No. 86820R.
(46) Thakur, N.; Giuliani, A.; Nahon, L.; Castellanos, S. Photon-induced fragmentation of zinc-based oxoclusters for EUV lithography applications. *J. Photopolym. Sci. Technol.* **2020**, *33* (2), 153−158.
(47) Richards, P. G.; Torr, D. G. An investigation of the consistency of the ionospheric measurements of the photoelectron flux and solar EUV flux. *J. Geophys. Res.: Space Phys.* **1984**, *89* (A7), 5625−5635.
(48) Chen, Y.-J.; Nuevo, M.; Yeh, F.-C.; Yih, T.-S.; Sun, W.-H.; Ip, W.-H.; Fung, H.-S.; Lee, Y.-Y.; Wu, C.-Y. R. Infrared study of UV/EUV irradiation of naphthalene in H_2O+NH_3 ice. *Adv. Geosci.* **2007**, *7*, 79−91.

https://doi.org/10.1021/acsmaterialsau.4c00010
ACS Mater. Au 2024, 4, 468−478

(49) Ebel, K.; Bald, I. Low-energy (5−20 eV) electron-induced single and double strand breaks in well-defined DNA sequences. *J. Phys. Chem. Lett.* **2022**, *13* (22), 4871−4876.
(50) Cardineau, B.; Del Re, R.; Al-Mashat, H.; Marnell, M.; Vockenhuber, M.; Ekinci, Y.; Sarma, C.; Neisser, M.; Freedman, D. A.; Brainard, R. L. EUV resists based on tin-oxo clusters. *Proc. SPIE* **2014**, *9051*, No. 90511B.
(51) Haitjema, J.; Wu, L.; Giuliani, A.; Nahon, L.; Castellanos, S.; Brouwer, A. M. UV and VUV-induced fragmentation of tin-oxo cage ions. *Phys. Chem. Chem. Phys.* **2021**, *23* (37), 20909−20918.
(52) Ma, J. H.; Needham, C.; Wang, H.; Neureuther, A.; Prendergast, D.; Naulleau, P. mechanistic advantages of organotin molecular EUV photoresists. *ACS Appl. Mater. Interfaces.* **2022**, *14* (4), 5514−5524.
(53) Vollenbroek, F. A.; Spiertz, E. J.; Photoresist systems for microlithography. In *Electronic Applications*; Springer Nature, 2005, pp 85−111.
(54) *X-ray Properties of the Elements*; CXRO, 1995. https://henke.lbl.gov/optical_constants/pert_form.html (accessed Dec 15, 2023).
(55) Fallica, R.; Haitjema, J.; Wu, L.; Castellanos, S.; Brouwer, F.; Ekinci, Y. Absorption coefficient and exposure kinetics of photoresists at EUV. *Proc. SPIE* **2017**, *10143*, No. 101430A.
(56) Nandi, S.; Khillare, L.; Kumar, S.; Moinuddin, M. G.; Chauhan, M.; Choudhary, S.; Sharma, S. K.; Ghosh, S.; Gonsalves, K. E. Induced chemical networking of organometallic tin in a cyclic framework for sub-10 nm patterning and iterconnect application. *ACS Appl. Nano Mater.* **2023**, *6* (6), 4132−4140.
(57) Gajewska, M.; Luzyanin, K. V.; Guedes da Silva, M. F. C.; Li, Q.; Cui, J.; Pombeiro, A. J. Cyclic trinuclear diorganotin (IV) complexes−the first tin compounds bearing oximehydroxamate ligands: synthesis, structural characterization and high in vitro cytotoxicity. *Eur. J. Inorg. Chem.* **2009**, *2009* (25), 3765−3769.
(58) Deng, W.; Zhang, L.; Li, L.; Chen, S.; Hu, C.; Zhao, Z.-J.; Wang, T.; Gong, J. Crucial Role of surface hydroxyls on the activity and stability in electrochemical CO_2 reduction. *J. Am. Chem. Soc.* **2019**, *141* (7), 2911−2915.
(59) Mattson, E. C.; Cabrera, Y.; Rupich, S. M.; Wang, Y.; Oyekan, K. A.; Mustard, T. J.; Halls, M. D.; Bechtel, H. A.; Martin, M. C.; Chabal, Y. J. Chemical modification mechanisms in hybrid hafnium oxo-methacrylate nanocluster photoresists for extreme ultraviolet patterning. *Chem. Mater.* **2018**, *30* (17), 6192−6206.
(60) Oleksak, R. P.; Ruther, R. E.; Luo, F.; Amador, J. M.; Decker, S. R.; Jackson, M. N.; Motley, J. R.; Stowers, J. K.; Johnson, D. W.; Garfunkel, E. L. Evaluation of thermal and radiation induced chemistries of metal oxo−hydroxo clusters for next-generation nanoscale inorganic resists. *ACS Appl. Nano Mater.* **2018**, *1* (9), 4548−4556.
(61) Frederick, R. T.; Saha, S.; Diulus, J. T.; Luo, F.; Amador, J. M.; Li, M.; Park, D.-H.; Garfunkel, E. L.; Keszler, D. A.; Herman, G. S. Thermal and radiation chemistry of butyltin oxo hydroxo: A model inorganic photoresist. *Microelectron. Eng.* **2019**, *205*, 26−31.
(62) Sahana, R.; Mounica, P.; Ramya, K.; Arivazhagan, G. Multimers of 1-propanol and their heteromolecular hydrogen bonds with ethyl acetate: fourier transform infrared spectral studies. *J. Solution Chem.* **2023**, *52*, 1396−1414.
(63) Zuo, P.; Cao, S.; Jiao, J.; Xiang, Q.; Men, J.; Wang, R. The adsorption performances of salicylhydroxamic acid-functionalized polystyrene-grafted SiO_2 particles toward quercetin. *J. Macromol. Sci., Part A. Pure Appl. Chem.* **2020**, *57* (12), 800−809.
(64) Ricci, C.; Bleay, S.; Kazarian, S. G. Spectroscopic imaging of latent fingermarks collected with the aid of a gelatin tape. *Anal. Chem.* **2007**, *79* (15), 5771−5776.
(65) Palaniappan, P. R.; Pramod, K. The effect of titanium dioxide on the biochemical constituents of the brain of Zebrafish (Danio rerio): An FT-IR study. *Spectrochim. Acta, Part A* **2011**, *79* (1), 206−212.
(66) Tian, M.; Gao, Z.; Ji, B.; Fan, R.; Liu, R.; Chen, P.; Sun, W.; Hu, Y. Selective flotation of cassiterite from calcite with salicylhydroxamic acid collector and carboxymethyl cellulose depressant. *Minerals* **2018**, *8* (8), 316.
(67) Miao, Y.; Wen, S.; Feng, Q.; Liao, R. Enhanced adsorption of salicylhydroxamic acid on ilmenite surfaces modified by fenton and its effect on floatability. *Colloids Surf., A* **2021**, *626*, No. 127057.
(68) Hanif, M.; Arshad, J.; Astin, J. W.; Rana, Z.; Zafar, A.; Movassaghi, S.; Leung, E.; Patel, K.; Söhnel, T.; Reynisson, J. A multitargeted approach: organorhodium anticancer agent based on vorinostat as a potent histone deacetylase inhibitor. *Angew. Chem., Int. Ed.* **2020**, *59* (34), 14609−14614.
(69) Lockhart, T. P.; Manders, W. F. Structure determination by NMR spectroscopy. Dependence of $|^2J$ (^{119}Sn, ^{1}H)| on the Me-Sn-Me angle in methyltin (IV) compounds. *Inorg. Chem.* **1986**, *25* (7), 892−895.
(70) Holeček, J.; Nadvornik, M.; Handlíř, K.; Lyčka, A. ^{13}C and ^{119}Sn NMR spectra of Di-n-butyltin (IV) compounds. *J. Organomet. Chem.* **1986**, *315* (3), 299−308.
(71) Lautié, A.; Froment, F.; Novak, A. Relationship between NH stretching frequencies and N··· O distances of crystals containing NH··· O hydrogen bonds. *Spectrosc. Lett.* **1976**, *9* (5), 289−299.
(72) Yin, H.; Dong, L.; Hong, M.; Cui, J. Structural diversity of organotin (IV) complexes self-assembled from hydroxamic acid and mono-or dialkyltin salts. *J. Organomet. Chem.* **2011**, *696* (9), 1824−1833.
(73) Diulus, J. T.; Frederick, R. T.; Hutchison, D. C.; Lyubinetsky, I.; Addou, R.; Nyman, M.; Herman, G. S. Effect of ambient conditions on radiation-induced chemistries of a nanocluster organotin photoresist for next-generation EUV nanolithography. *ACS Appl. Nano Mater.* **2020**, *3* (3), 2266−2277.
(74) Amanullah, F. M.; Pratap, K. J.; Hari Babu, V. Compositional analysis and depth profile studies on undoped and doped tin oxide films prepared by spray technique. *Mater. Sci. Eng. B.* **1998**, *52* (2), 93−98.
(75) Cheng, P.; Lv, L.; Wang, Y.; Zhang, B.; Zhang, Y.; Zhang, Y.; Lei, Z.; Xu, L. $SnO_2/ZnSnO_3$ double-shelled hollow microspheres based high-performance acetone gas sensor. *Sens. Actuators, B* **2021**, *332*, No. 129212.
(76) Yu-de, W.; Chun-lai, M.; Xiao-dan, S.; Heng-de, L. Preparation and characterization of SnO2 nanoparticles with a surfactant-mediated method. *Nanotechnology* **2002**, *13* (5), 565.
(77) Junzo, O.; Tomoya, H.; Yotaro, K.; Rokuro, O. ^{119}Sn, ^{13}C, and ^{1}H NMR studies on six-coordinate dimethyltin bis(chelate) compounds. *Chem. Lett.* **1981**, *10* (2), 273−274.
(78) Otera, J. ^{119}Sn chemical shifts in five- and six-coordinate organotin chelates. *J. Organomet. Chem.* **1981**, *221* (1), 57−61.
(79) Bhattarai, S.; Chao, W.; Aloni, S.; Neureuther, A.; Naulleau, P. Analysis of shot noise limitations due to absorption count in EUV resists. *Proc. SPIE* **2015**, *9422*, No. 942209.
(80) Mojarad, N.; Gobrecht, J.; Ekinci, Y. Beyond EUV lithography: a comparative study of efficient photoresists' performance. *Sci. Rep.* **2015**, *5* (1), 9235.
(81) Buitrago, E.; Nagahara, S.; Yildirim, O.; Nakagawa, H.; Tagawa, S.; Meeuwissen, M.; Nagai, T.; Naruoka, T.; Verspaget, C.; Hoefnagels, R.; et al. Sensitivity enhancement of chemically amplified resists and performance study using EUV interference lithography. *Proc. SPIE* **2016**, *9776*, No. 97760Z.
(82) Vesters, Y.; McClelland, A.; De Simone, D.; Popescu, C.; Dawson, G.; Roth, J.; Theis, W.; Vandenberghe, G.; Robinson, A. P. Multi-trigger resist patterning with ASML NXE3300 EUV scanner. *Proc. SPIE* **2018**, *10583*, No. 1058308.
(83) O'Callaghan, G.; Popescu, C.; McClelland, A.; Kazazis, D.; Roth, J.; Theis, W.; Ekinci, Y.; Robinson, A. P. Multi-trigger resist: novel synthesis improvements for high resolution EUV lithography. *Proc. SPIE* **2019**, *10960*, No. 109600C.
(84) Shirotori, A.; Vesters, Y.; Hoshino, M.; Rathore, A.; De Simone, D.; Vandenberghe, G.; Matsumoto, H. Development of main chain scission type photoresists for EUV lithography. *Proc. SPIE* **2019**, *11147*, No. 111470J.

https://doi.org/10.1021/acsmaterialsau.4c00010
ACS Mater. Au 2024, 4, 468−478

(85) Stowers, J.; Telecky, A.; Kocsis, M.; Clark, B.; Keszler, D.; Grenville, A.; Anderson, C.; Naulleau, P. Directly patterned inorganic hardmask for EUV lithography. *Proc. SPIE* **2011**, *7969*, No. 796915.
(86) Ekinci, Y.; Vockenhuber, M.; Terhalle, B.; Hojeij, M.; Wang, L.; Younkin, T. Evaluation of resist performance with EUV interference lithography for sub-22-nm patterning. *Proc. SPIE* **2012**, *8322*, No. 83220W.
(87) Trikeriotis, M.; Krysak, M.; Chung, Y. S.; Ouyang, C.; Cardineau, B.; Brainard, R.; Ober, C.; Giannelis, E.; Cho, K. A new inorganic EUV resist with high-etch resistance. *Proc. SPIE* **2012**, *8322*, No. 83220U.
(88) Chakrabarty, S.; Sarma, C.; Li, L.; Giannelis, E.; Ober, C. Increasing sensitivity of oxide nanoparticle photoresists. *Proc. SPIE* **2014**, *9048*, No. 90481C.
(89) Ober, C.; Jiang, J.; Zhang, B.; Li, L.; Giannelis, E.; Chun, J. S.; Neisser, M.; Sierra-Alvares, R. New developments in ligand-stabilized metal oxide nanoparticle photoresists for EUV lithography. *Proc. SPIE* **2015**, *9422*, No. 942207.
(90) De Simone, D.; Kljucar, L.; Das, P.; Blanc, R.; Beral, C.; Severi, J.; Vandenbroeck, N.; Foubert, P.; Charley, A.; Oak, A.; et al. 28nm pitch single exposure patterning readiness by metal oxide resist on 0.33NA EUV lithography. *Proc. SPIE* **2021**, *11609*, No. 116090Q.
(91) Del Re, R.; Passarelli, J.; Sortland, M.; Cardineau, B.; Ekinci, Y.; Buitrago, E.; Neisser, M.; Freedman, D.; Brainard, R. Low-line edge roughness extreme ultraviolet photoresists of organotin carboxylates. *J. Micro/Nanolithogr., MEMS, MOEMS* **2015**, *14* (4), No. 043506.
(92) Wilklow-Marnell, M.; Moglia, D.; Steimle, B.; Cardineau, B.; Al-Mashat, H.; Nastasi, P.; Heard, K.; Aslam, A.; Kaminski, R.; Murphy, M.; et al. First-row transitional-metal oxalate resists for EUV. *J. Micro/Nanolithogr., MEMS, MOEMS* **2018**, *17* (4), No. 043507.
(93) Maruyama, K.; Shimizu, M.; Hirai, Y.; Nishino, K.; Kimura, T.; Kai, T.; Goto, K.; Sharma, S. Development of EUV resist for 22nm half pitch and beyond. *Proc. SPIE* **2010**, *7636*, No. 76360T.
(94) Putna, E. S.; Younkin, T.; Chandhok, M.; Frasure, K. EUV lithography for 30nm half pitch and beyond: exploring resolution, sensitivity, and LWR tradeoffs. *Proc. SPIE* **2009**, *7273*, No. 72731L.
(95) Kim, H.-W.; Na, H.-S.; Cho, K.-Y.; Park, C.-M.; Yasue, T.; Mayya, S.; Cho, H.-K. Patterning with EUVL: the road to 22nm node. *Proc. SPIE* **2010**, *7636*, No. 76360Q.
(96) Zhang, P. Monte carlo simulation on the CD-SEM Images of SiO_2/Si systems. *Microsc. Microanal.* **2019**, *25* (4), 849−858.
(97) Bunday, B.; Allgair, J.; Adan, O.; Tam, A.; Latinski, S.; Eytan, G. Small feature accuracy challenge for CD-SEM metrology physical model solution. *Proc. SPIE* **2006**, *6152*, No. 61520S.
(98) Naulleau, P. Chapter 5 - EUV lithography patterning challenges. *Front. Nanosci.* **2016**, *11*, 177−192.
(99) Grube, M.; Schille, B.; Schirmer, M.; Gerngroß, M.; Hübner, U.; Voigt, P.; Brose, S. Medusa 82—Hydrogen silsesquioxane based high sensitivity negative-tone resist with long shelf-life and grayscale lithography capability. *J. Vac. Sci. Technol. B* **2021**, *39* (1), No. 012602.
(100) Shen, J.; Aydinoglu, F.; Soltani, M.; Cui, B. E-beam lithography using dry powder resist of hydrogen silsesquioxane having long shelf life. *J. Vac. Sci. Technol. B* **2019**, *37* (2), No. 021601.

https://doi.org/10.1021/acsmaterialsau.4c00010
ACS Mater. Au 2024, 4, 468−478